J Mater Sci (2023) 58:740–756

Ceramics

High performance nano hydroxyapatite coating on zinc for biomedical applications

Madiha A. Shoeib[1] and Soha A. Abdel-Gawad[2,*]

[1] *Corrosion Control & Surface Protection Department, Central Metallurgical Research and Development Institute, CMRDI, Cairo, Egypt*

[2] *Chemistry Department, Faculty of Science, Cairo University, Giza, Egypt*

Received: 15 September 2022
Accepted: 28 November 2022
Published online: 1 January 2023

ABSTRACT

Zinc and its alloys have been given promising consideration as a new biodegradable implant for use in the human body. Compact and uniform nano hydroxyapatite coatings containing chitosan were successfully deposited onto zinc substrate in an aqueous solution utilizing microwave-assisted process in about 10 min. The quick composite coatings are derived by microwave heating compared with the coatings derived by electrodeposition. The as-deposited coatings formed by electrodeposition synthesis were known as brushite, which was converted to hydroxyapatite after 1 h of immersion (post treated) in 1 M aqueous sodium hydroxide solutions at 100 °C. The incorporation of chitosan (from 0.01–0.05 g/l) into the coating composition results in a smooth and uniform coating structure. SEM, EDS, and an X-ray diffractometer were utilized to analyze coated samples' surfaces to evaluate their surface morphology, chemical composition, and crystalline structures. The in vitro degradation behavior of the composite-coated samples in simulated body fluid at pH 7.4 and 37 °C was evaluated using electrochemical impedance spectroscopy and potentiodynamic polarization. The outcomes showed that microwave-derived coatings provided superior corrosion resistance for zinc implants as compared to electrodeposited coatings. Furthermore, the use of chitosan in hydroxyapatite coatings increased electrochemical corrosion performance. Low chitosan concentrations (0.01–0.03 g/l) exhibit superior anti-corrosion properties than higher concentrations (0.05 g/l). Against Staphylococcus aureus, the coatings demonstrated strong antibacterial efficacy. These corrosion outcomes and the fruitful deposition of a hydroxyapatite/chitosan composite coating on zinc substrate indicate that the coating is efficient for the creation of new composite coatings for either functional implants or regenerative medicine. The resultant coating may be an excellent option for bone implants.

Handling Editor: Catalin Croitoru.

Address correspondence to E-mail: Soha.gawad@cu.edu.eg; Soha.gawad@yahoo.com

https://doi.org/10.1007/s10853-022-08034-6

Introduction

Zinc and its alloys have a hopeful future as new biodegradable implants in the human body because of their biological benefits, acceptable degradation rate, and degradation behavior [1, 2]. A zinc-based medical implant is totally absorbed into the body. An alternative that can even avoid the need for follow-up surgery, saves money and, more importantly, benefits the patient by removing the risk of anaesthesia or infections [3, 4]. Zinc is a vital trace element in the human body that is involved in a variety of cellular functions [5–7]. Zinc implants have minimal corrosion rates and the main corrosion byproduct, Zn^{2+}, is well regulated within physiological systems and below the recommended dietary allowance (RDA) limit for the majority of medical applications [8, 9]. Zinc's biological benefits meet the criteria for necessary biodegradable metals. As candidates for biodegradable metallic materials, Mg and Fe have been investigated as candidates for biodegradable metallic materials [10]. Although Mg and its alloys corrode rapidly and are related to the formation of hydrogen gas [11–13], Fe and its alloys corrode too slowly and the corrosion products reject adjacent cells and biological matrix [14, 15]. According to thermodynamic opinion, Zn has a standard electrode potential between Fe and Mg, namely Mg (2.37 V), Zn (0.763 V), and Fe (0.440 V) (all V values vs. SHE) [16]. It is indicated that zinc has a moderate corrosion rate in compliance with clinical requirements. The release of metal ions from medical implants results in inflammatory effects in the physiological system. Surface treatment and modification enhance the biodegradability of zinc implants. Because of this, bioactive coatings like chitosan (CS) and hydroxyapatite (HA) are some of the best bioactive biomaterials for making bone [17, 18].

Calcium phosphate is the most common inorganic component of hard biological tissues [19, 20]. It is found in bones and teeth as hydroxyapatite (HA), with the formula $Ca_{10}(PO_4)_6(OH)_2$ at near-neutral pH, but brushite ($CaHPO_4.2H_2O$) or monetite ($CaHPO_4$) are more stable under acidic conditions [21]. HA coating and/or deposition of metal alloys helps to osseointegrate implants and increases the direct binding of implants to the bone [22, 23]. Techniques for depositing hydroxyapatite on metal implantation surfaces include spin coating, plasma spraying, sputtering, sol–gel coating, electrophoretic coating, and electrodeposition [24–26]. Using the electrodeposition method can prevent unintended phase changes since it operates at a low temperature and can deposit an intricate architectural coating with a precise thickness [27]. The microwave assisted coating method was successfully used to uniformly coat a dense HA layer onto a zinc substrate in a short time, thus enhancing their bioactivity and/or biocompatibility. Currently, the microwave-assisted hydroxyapatite processing method has marked advantages over conventional methods [28]. It decreases the reaction time very substantially by optimizing energy transmission inside the volume, allows reproducibility, produces uniform particle size and provides high yield and crystallinity [29–32]. Recently, scientists have tried to strengthen the adhesive, structural, and physicochemical qualities of implant materials coated with HA [33, 34]. The importance of adding additives to the deposition solution, such as polymers, was highlighted [35]. Chitosan is a naturally occurring cationic polysaccharide shaped by the alkaline N-deacetylation of chitin. It offers remarkable features that make it perfect for use in biomedical implants, including antibacterial functionality, high chemical stability, biocompatibility, biodegradability, and enhanced mechanical properties. Chitosan is a hemostatic material that aids in bone and wound healing [36].

The aim of this study is to deposit a nano HA/CS composite coating on zinc substrate by a microwave assisted method and compare it with coatings derived by electrodeposition. The in vitro degradation behavior and antibacterial performance of nano composite coatings on zinc for clinical (bone implant) applications have been evaluated. The novelty of this research is mainly consisting in the synthesis of nano structure HA/CS coating by simple fast and low-cost method on zinc substrate which is candidate metal for biodegradable implant. The HA/CS coating enhance the bone healing due to improve corrosion resistance and antibacterial properties. The HA coating on zinc is quiet not fully revealment and require to be studies.

Materials and methods

Electrode preparation

Zinc has been used as a metallic substrate (area = 0.385 cm^2). Inductively coupled plasma atomic-emission spectroscopy (ICP-AES) was utilized to determine the chemical composition of the zinc, as shown in Table 1 (wt.%). The sample disc measured 6 mm in diameter and 2 mm in thickness. A Teflon-coated stainless-steel rod was used to hold each disc to provide total isolation. The discs were mechanically polished with SiC sheets up to 2400 grit, rinsed in triple-distilled water, and then cleaned in an acetone-containing ultrasonic bath for five minutes at room temperature. In order to eliminate zinc oxide and make the substrates rougher for better adhesion, the Zn substrates were etched in a 0.1M HCl solution for 1 min. Before the next step, the samples were cleaned with distilled water and left to dry [37, 38].

Chemical and reagents

Chitosan (medium molecular weight) with a deacetylation of 75–85%, glacial acetic acid (99.0%), calcium nitrate, anhydrous monobasic ammonium phosphate, ammonium hydroxide, and sodium hydroxide pellets (each chemical constituent was acquired from Aldrich Company). Analar (grade reagents), as well as triply distilled water used.

Coatings preparation

The coating solution was created by combining 0.21 M Ca $(NO_3)_2$ and 0.125 M $NH_4H_2PO_4$ in an aqueous solution with a pH of 3.6–4 and a Ca/P ratio of 1.67. The chitosan electrolyte solution was created by dissolving 0.4 gm of chitosan powder in 100 ml of dilute acetic acid (1% w/w) and stirring for 5 h at room temperature to get a clear solution. The pH was buffered to 3.7 using Tris-buffer. For the deposition of the hydroxyapatite/chitosan composite layer, different amounts of chitosan solution, ranging from 0.01–0.05 g/l, were added to the coating solution. The electrodeposition current density was 2 mA/cm^2 and 90 rpm magnetic stirring was conducted for 3600 s [39–41]. The electrodeposition was carried out at room temperature in an electric cell with three selective electrodes; a zinc disc as the working electrode (cathode), a platinum basket as the counter electrode (anode), and an Ag/AgCl electrode as the reference electrode. For the coating synthesized by domestic microwave (Samsung ME711K, 2450 MHz, 1150 W, OM75S Magnetron). In all the experiments, the microwave irradiation power (600 W) was employed for 10 min. The pH of the solution was attuned to 7 using 1 M NH_4OH. The treated samples were submerged in a 100 ml coating solution in a Teflon lined beaker. The solution mixture was microwave irradiated for 10 min. The coated zinc discs were cleaned with deionized water and dried for 24 h at room temperature. Finally, for hydrothermal treatment, the prepared samples by electrodeposition were immersed in 1 M NaOH solution at 100 °C for 1 h, then washed with distilled water and dried in air [42, 43]. PosiTector 6000 is used to measure coating thickness.

Surface characterization

Surface morphologies of coatings and elemental analyses of the deposited coating were studied utilizing a scanning electron microscope (JEOL-JSM-5410, Japan) armed with an energy dispersive spectrometer unit (EDS-Oxford). The phase analysis of the coating was determined using an X-ray diffractometer (Bruker AXS-D8, Advance, Germany, operated at 35 kV and 45 mA with CuKα radiation λ = 0.1540 nm). The coating's nanocrystalline size was calculated using Scherrer's equation.

$$D = k\lambda/\beta\cos\theta \quad (1)$$

where D is the average crystal size, k is the Scherrer's constant, which is 0.94, λ is the X-ray source's wave length (0.154 nm for CuKα radiation), β is the peak width at half its maximum, and θ is the diffraction angle [44, 45].

Electrochemical test

At 37 °C, electrochemical measurements were achieved (potentiostat/Galvanostat, Auto lab

Table 1 The chemical composition of zinc substrate (in weight percentages)

Zn	Pb	Fe	Cr	V	Ca	Si	Ce	Sb	Mo	Sn	W	Al
98.443	0.031	0.038	0.013	0.065	0.182	0.62	0.011	0.011	0.003	0.005	0.492	0.086

PGSTAT 302 N, Netherlands) in simulated body fluid solution containing (g/l) NaCl 8, $CaCl_2$ 0.14, KCl 0.4, $NaHCO_3$ 0.35, $C_6H_{12}O_6$ 1, NaH_2PO_4 0.1, $MgCl_2$ $_{0.6}H_2O$ 0.1, Na_2HPO_4 $0.2H_2O$ 0.06 and $MgSO_4$ $0.7H_2O$ 0.06.at pH 7.4 [46–48]. A three-electrode cell containing 100 mL SBF was utilized, with an Ag/AgCl as the reference electrode, a platinum counter electrode, and Zn or coated-Zn substrates serving as the working electrodes. Before beginning the potentiodynamic measurements, the open-circuit potentials (OCP) were stabilized for 30 min. A perturbation amplitude of 5 mV was used during (EIS) in the frequency range of 10 MHz–100 kHz. Potentiodynamic polarization curves between − 1.6 mV and − 0.2 mV were performed at a scan rate of 1 mV/s.

Antibacterial activity

Using nutritional agar medium, the antibacterial activity of two samples coated with microwave-produced hydroxyapatite and hydroxyapatite/chitosan composite coatings was evaluated against Staphylococcus aureus (Gram positive bacterium). Ampicillin was a common medication for gram-positive bacteria. As a solvent control, DMSO was employed.

Results and discussion

Phase structure of the coating

The following electrochemical deposition reactions were used to create the composite coatings brushite/chitosan on the surface of zinc [49, 50].

First, when water is reduced at the surface of the implant, hydrogen gas and hydroxide ions are produced.

$$2H_2O + 2e \leftrightarrow H_2 + 2OH^- \quad (2)$$

According to equilibrium, the hydroxide ions produced could react with di hydrogen phosphate.

$$H_2PO_4^- + OH^- \leftrightarrow H_2O + HPO_4^{2-} \quad (3)$$

A stoichiometric precipitation of brushite occurred.

$$Ca^{2+} + HPO_4^{2-} + 2H_2O \leftrightarrow CaHPO_4 \cdot 2H_2O \quad (4)$$

In acetic acid, chitosan was easily dissolved. At a low pH of 3.7, chitosan becomes a cationic poly electrolyte [51–54].

$$Chit\text{-}NH_2 + 3H_3O^+ \rightarrow Chit\text{-}NH_3^+ + H_2O \quad (5)$$

The charged chitosan is propelled toward the cathodic surface by the electric field, where it releases its charge and deposits an insoluble substance.

$$Chit\text{-}NH_3^+ + OH^- \rightarrow Chit\text{-}NH_2 + H_2O \quad (6)$$

The as-deposited coating is primarily composed of dicalcium phosphate dihydrate (DCPD, brushite). The conversion to HA was carried out in a 1 M NaOH solution at 100 °C for 1 h.

At pH 6.5–7.0, calcium and phosphate ions were present in the initial solution and deposited on the substrate. Simultaneously, the hydroxyapatite production occurs on substrate surface [17].

$$10Ca^{2+} + 6\ H_2PO_{4^-} + 14OH\text{-} \rightarrow Ca_{10}(PO_4)_6(OH)_2 + 12H_2O \quad (7)$$

Microwave irradiation revealed a direct precipitation of nano-HA. Microwave energy activates a rapid ionic interaction including Ca^{2+}, OH^-, and PO_4^{2-} ions, resulting in precipitation of the stable HA [29]. Reaction (7) shows how HA is made using microwave irradiation, which is a fast way to get nano-sized HA particles on a zinc substrate.

Figure 1(a), (b) shows X-ray diffraction patterns of the HA coating and HA/CS coating prepared by the electrodeposition method. The gotten data suggested that the coating layer is composed of highly crystalline HA with main diffraction peaks observed at 2Θ = 36.2°, 38.9°, 43.1° and 54.2° and in HA/CS composite coating, a peak at 2Θ = 12°, 20° is observed for chitosan (the peak strength of CS in composite coatings was not significant because of the large difference in the intensity of the diffraction peaks between HA and CS, and the low amount of CS in HA coatings). In composite coatings, the intensity of typical HA peaks decreased, indicating that a CS layer forms on the surface of the HA coating [55]. Evidently, these results were good in agreement with standard ICDD cards 01-076-0694.Fig. 1 (inset) The X-ray pattern of the main brushite peaks at 2Θ = 28.4°, 35.8°, 47.6° and 55.2° with standard ICDD cards (00-009-0077).Fig. 2(a), (b) shows X-ray diffraction patterns of the HA coating and HA/CS coating derived by the microwave assisted method, which is very similar to the electrodeposited coat, but the peak width and relative intensity for diffraction peaks confirm that the produced coating is more

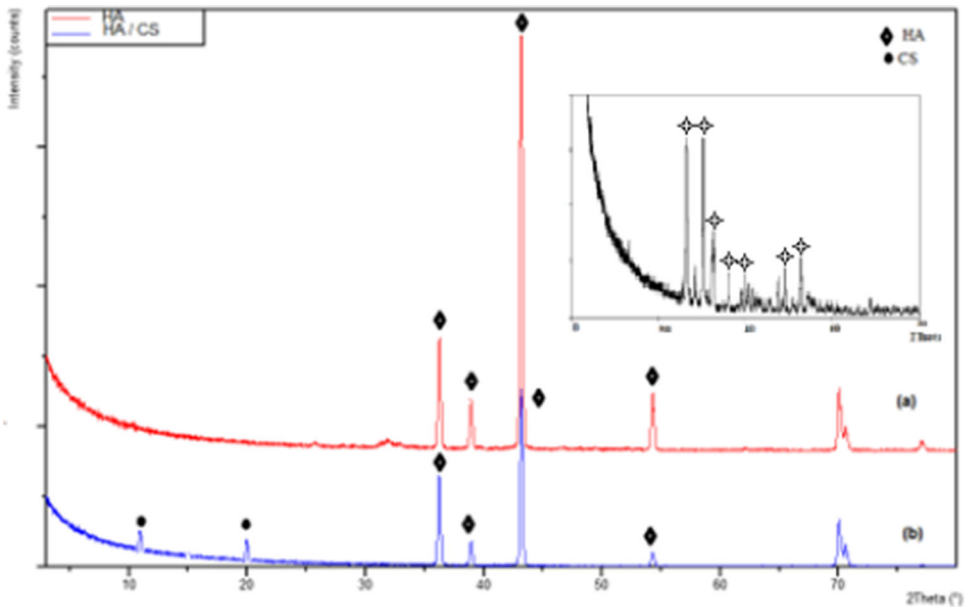

Figure 1 X-ray diffraction pattern of HA (**a**) and (**b**) HA/CS (0.03 g/l) electrodeposition coatings. Inset X-ray diffraction pattern of brushite (✧).

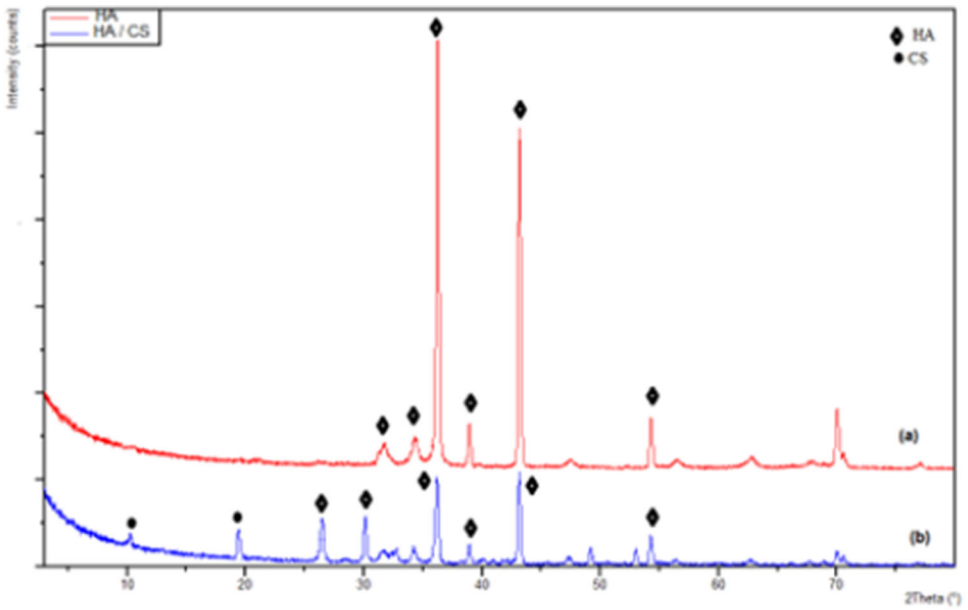

Figure 2 X-ray diffraction pattern of HA (**a**) and (**b**) HA/CS (0.03 g/l) microwave coatings.

Table 2 XRD analysis results (nanocrystalline size) of HA and HA/CS(0.03 g/l) composite coatings

	Electrodeposition		Microwave	
	Peak position (2θ)	Crystallite size(nm)	Peak position (2θ)	Crystallite size(nm)
HA	36.2°	67.9	36.1°	70.6
	38.9°	49.9	38.8°	72.5
	43.1°	50.5	43.0°	79.3
	54.3°	64.8	54.1°	65.5

dense with high crystallinity [49, 56]. Table 2 displays the estimated sizes of crystallites.

Microstructure characterization

However, the produced coatings having the same phase composition, but the morphologies of HA coatings arranged by electrodeposited and microwave techniques were significantly different. Figure 3(a–d) depicts the surface morphology of coatings created using the electrodeposition method. The SEM image was represented with higher magnifications; a uniform distribution of coatings was observed in all samples. Figure 3(a, b) shows SEM images of electrodeposited brushite and brushite/CS (0.03 g/l) coating, respectively, on zinc substrate at a constant current density of 2 mA/cm^2 for 3600 s. It is clear that a typical brushite structure was observed, and the composite coatings are more ordered as CS fills the interstitial voids. Figure 3(c, d) shows the same coating after hydrothermal treatment in 0.1 M NaOH at 100 °C for 1 h to convert it to HA and HA/CS. The HA coating obtained by the electrodeposition method was instituted by a homogenous plate-like structure and the thickness of the coating was ~ 10 ± 2 µm.

Figure 4(a, b) demonstrates the surface morphologies of the HA and HA/CS (0.03 g/l) nano coatings synthesized by microwave irradiation on zinc substrate. At high magnification, Fig. 4(a) shows rod-like HA crystals which piled up to form a flower-like structure. The thickness of the coating was ~ 14 ± 2 µm. The surface morphology of the composite HA/CS coatings is shown in Fig. 4(b). The co-deposition of composite CS resulted in more adherent and compact coatings on the zinc substrate. In fact, chitosan acts as a bioadhesive enhancing the connection between HA particles and the zinc surface [49].

In principle, two stages, nucleation and crystal growth, are involved in the precipitation of HA coatings from aqueous solutions [56, 57]. As the solution's temperature and pH rise, these reactions become more powerful [58]. Low driving force elevates the interface to rise and travel laterally, leading to face-by-face growth and the acquired HA's morphology looking like a plate. High driving force, on the other hand, accelerates the interface's motion toward normal to itself, leading to spiral development and rod-like. In the electrodeposition strategy, the driving force was deemed insufficient; consequently, plate-like HA crystals were precipitated, then repeatedly coiled and agglomerated into enormous globules to lower the overall surface energy. The rod-like HA crystals were produced as a result of the interfacial development's driving force being boosted by microwave heating. Furthermore, the deposition procedure was accelerated, resulting in a thicker HA coating on the substrate, as a result of the higher HA nuclei transit rate in the solution under microwave irradiation [59].

Figure 3 **a**, **b** SEM images of electrodeposited brushite and brushite/CS (0.03 g/l) on zinc substrates, respectively; **c**, **d** the same coating after conversion to HA and HA/CS (0.03 g/l) with different magnifications. ▶

Figure 5 shows the cross-sectional of the HA coating on zinc substrate prepared by microwave-assisted method was ~ 14.83 µm which is in great consistent with the value measured by PosiTector 6000 device. The micrograph reveals that the coating is compact, dense and adheres on the surface.

Electrochemical test

The corrosion protection of a Zn substrate coated with brushite and brushite/CS composite coatings with different chitosan concentrations (0.01–0.05 g/l) was examined in SBF solution at 37 °C. Figure 6 presents the potentiodynamic polarization curves of the as-deposited coatings. The development of a protective layer by brushite and brushite/CS composite coatings improves surface resistance via shifting the corrosion potential in a positive direction and visibly reducing corrosion current density. Furthermore, the concentration of chitosan in the solution has a significant impact on coating quality. As the CS concentration rises to 0.03 g/l, the corrosion properties improve, which is linked to the creation of a dense, compact, and uniform layer at the surface. However, raising the concentration over 0.03 g/l reduces corrosion resistance because the solutions become viscous, preventing particles from moving to the zinc substrate and, as a result, reducing the uniformity and coherency of the composite coatings [47]. In this regard, Hahn et al. said that the compactness of the deposition in composite coatings is inversely related to the volume of chitosan [60].

Figure 7 shows the polarization curves of coated zinc after 1 h of immersion (post treatment) in 1 M

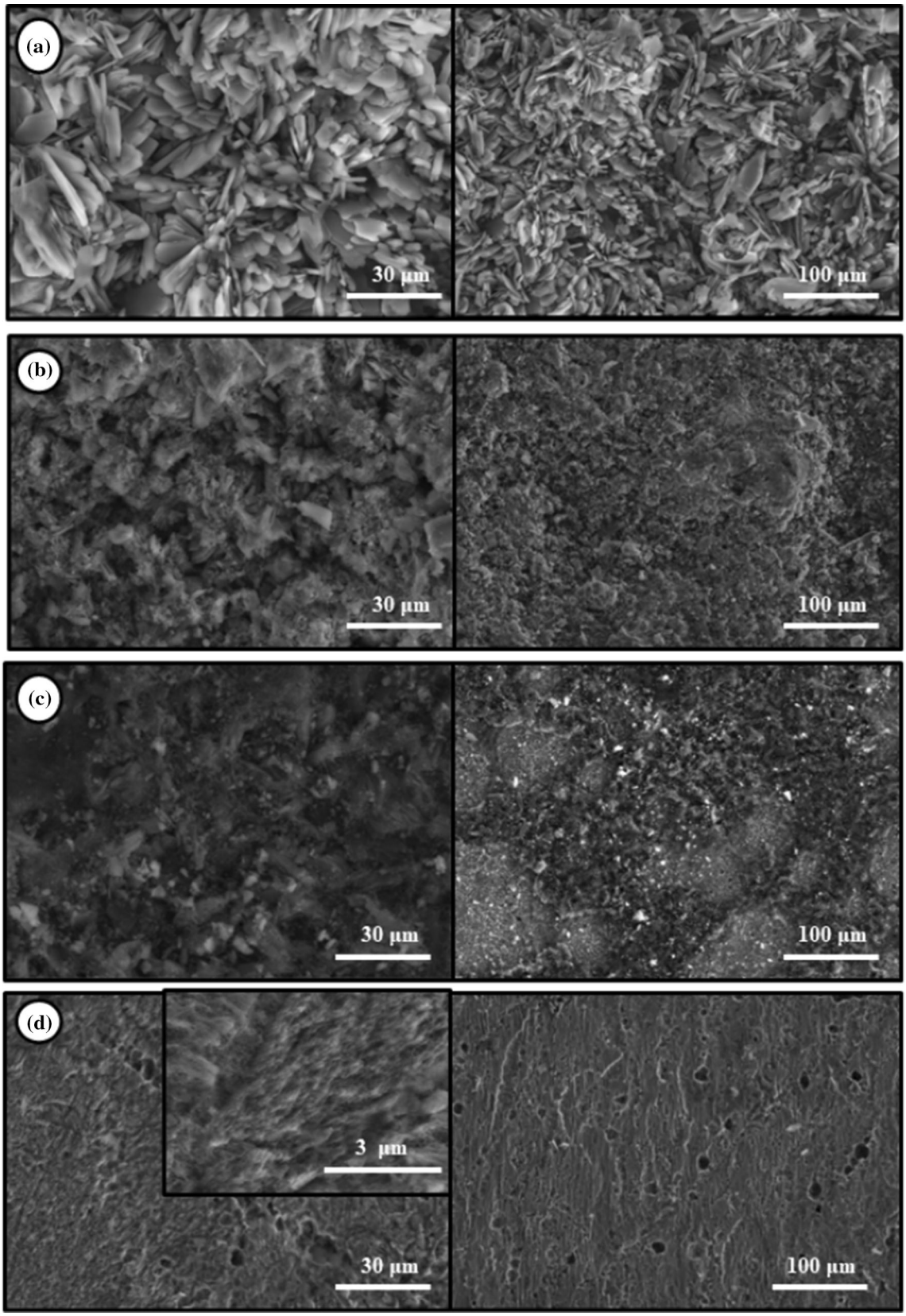
(a)
30 µm
100 µm
(b)
30 µm
100 µm
(c)
30 µm
100 µm
(d)
3 µm
30 µm
100 µm

aqueous sodium hydroxide solutions at 100 °C to assess the protective qualities of the HA and HA/CS composite coatings. In comparison to their as-deposited form, the corrosion current and rate of corrosion of the coated samples were dramatically reduced. The results show that composite coatings can protect zinc substrates and make them less likely to corrode in SBF environments. The anodic polarization curves credited to zinc dissolution $\left(Zn_{(S)} \rightarrow Zn^{2+}_{(aq)} + 2e^{-}\right)$ and the cathodic curves were assumed to hydrogen evolution $\left(2H_2O + 2e^{-} \rightarrow H_2 + 2OH^{-}_{(aq)}\right)$. Zinc ions have a propensity to create zinc hydroxide as the pH rises along with an increase in the generation of $\left(Zn^{2+}_{(aq)} + 2OH^{-}_{(aq)} \rightarrow Zn(OH)_{2(S)}\right)$ [61]. Solid $Zn(OH)_2$ is the primary corrosion product that precipitates on the zinc substrate's surface to prevent further corrosion. As a result of the aggressive chloride ions in the SBF competing with the $Zn(OH)_2$layer, soluble zinc chloride was formed $\left(Zn(OH)_2 + 2Cl^{-} \rightarrow ZnCl_2 + 2\,OH^{-}\right)$ Meanwhile, the presence of PO_4^{3-} and Ca^{2+} in the SBF solution reacted with OH^{-} favor the creation of hydroxyapatite e which offers secondary protection of zinc coated substrate [8]. The polarization resistance is known to be related to the corrosion current by the Stern–Geary equation via Tafel slopes [62].

$$R_p = \frac{\beta_a \beta_c}{2.3 I_{corr}(\beta_a + \beta_c)} \tag{8}$$

where (β_a and β_c) are the anodic and cathodic Tafel slopes.

The corrosion current density (i_{corr}) is related to the corrosion rate (R_i) by the following equation.

$$R_i = K i_{corr}(\mathrm{Eq} \cdot \mathrm{wt}\cdot)/d \tag{9}$$

where R_i is given in mm/y., i_{corr} in μA/cm^2, $K = 3.27 \times 10^{-3}$ mm g/μA cm y, Eq. wt. is the

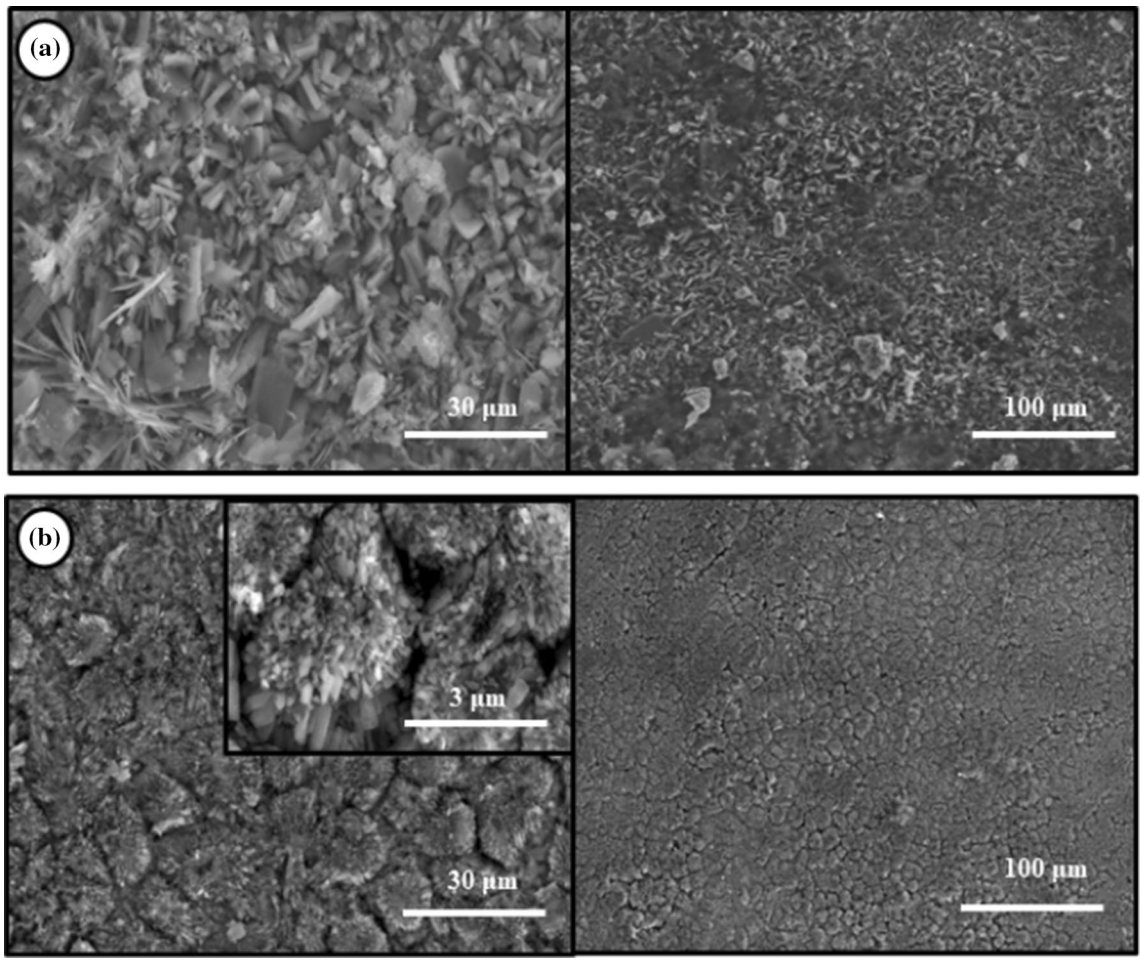

Figure 4 SEM images of **a** HA and **b** HA/CS (0.03 g/l) prepared using the microwave-assisted method with different magnifications.

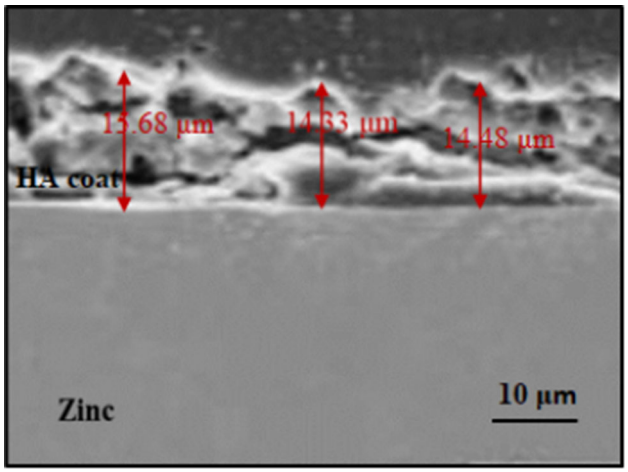

Figure 5 Cross-section of HA coating prepared by microwave-assisted method.

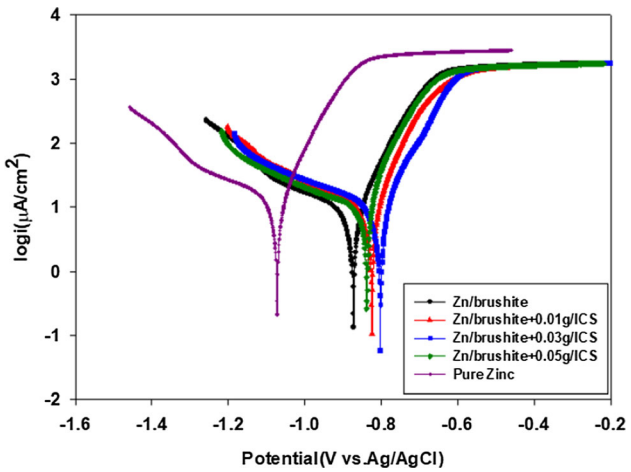

Figure 6 Potentiodynamic polarization curves of electrodeposited brushite and brushite /CS coatings on Zn substrate in SBF solution at 37 °C.

equivalent weight and d is the density of the zinc in g/cm^3 [45].

The corrosion protection efficiency (PE %) for zinc substrate nanocomposite coatings (investigated samples) immersed in SBF solution at 37 °C was calculated using the following equation [63].

$$\mathrm{PE}\% = 1 - i_{\mathrm{corr}}/i_{\mathrm{corr}^\circ} \times 100 \quad (10)$$

where i_{corr° and i_{corr} are the corrosion current densities of the zinc substrate before and after composite coatings, respectively. The corrosion characteristics determined from the polarization curves, including corrosion potential (E_{corr}), corrosion current density (I_{corr}), polarization resistance (R_p), corrosion rate (R_i)

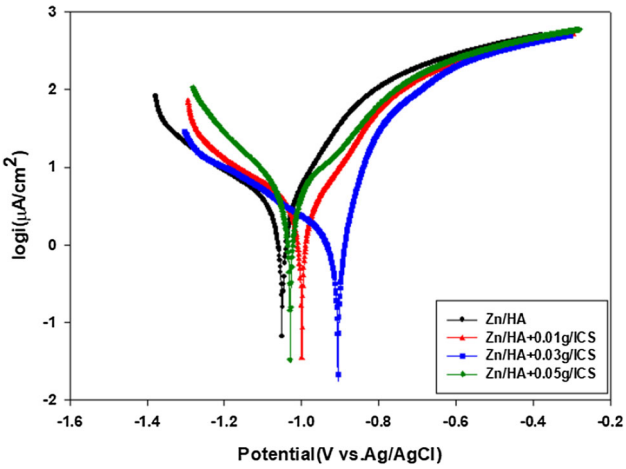

Figure 7 Potentiodynamic polarisation curves for coated zinc after 1 h of immersion (post treatment) in 1 M aqueous sodium hydroxide solutions at 100 °C and in SBF solutions at 37 °C.

and protection efficiency (PE %) are recorded in Table 3.

Utilizing EIS technique, the Nyquist and Bode plots of a zinc substrate coated with brushite and brushite/CS composite coating with different chitosan concentrations (0.01–0.05 g/l) was studied in SBF solution at 37 °C. The outcomes are presented in Fig. 8 and Fig. 9 for as-deposited brushite and brushite/CS and post-treated samples HA and HA/CS, respectively. The impedance investigation validates the polarization-based results that were previously obtained. The HA/CS coating has the best corrosion resistance, and the film's corrosion resistance increases as the CS concentration increases up to 0.03 g/l. One capacitive semicircular loop was found in the Nyquist plots. An increase in the semicircle's size and impedance indicates an increase in coating resistance in all cases. The simple model with a one-time constant, as shown in Fig. 10, is the well-fitting electric model to clarify the corrosion process. The equivalent circuit consists of a constant phase element (CPE) in series with the solution resistance *Rs*, which is parallel to the polarization resistance (charge transfer resistance) of the coated surface *Rp*. The constant phase element (CPE) compensates for the action of the capacitor due to the surface heterogeneity of the coating and is defined by its impedance value [64].

$$Z_{\mathrm{CPE}} = [C(j\omega)^{\alpha}]^{-1} \quad (11)$$

where α is a surface heterogeneity exponent, $0 \leq \alpha \leq 1$, j is an imaginary number ($j = (-1)^{1/2}$), $\omega = 2\pi f$ is

Table 3 Electrochemical parameters and corrosion rates obtained by polarization tests

Sample	E_{corr}/V	I_{corr}/μA/cm^2	Rp/KΩ	R_i/mm/y	PE%
Zinc	−1.07	13.7	0.69	0.41	–
Zn/ brushite	−0.87	6.5	0.76	0.32	53
Zn/brushite + 0.01 g/lCS	−0.82	5.2	0.85	0.25	62
Zn/brushite + 0.03 g/lCS	−0.80	4.4	0.93	0.17	68
Zn/brushite + 0.05 g/lCS	−0.84	5.8	0.83	0.31	58
Zn/HA	−1.05	3.1	2.01	0.30	77
Zn/HA + 0.01 g/lCS	−0.99	2.5	3.01	0.21	82
Zn/HA + 0.03 g/lCS	−0.90	1.1	4.70	0.03	92
Zn/HA + 0.05 g/lCS	−1.02	2.8	2.95	0.26	80
Microwave method					
Zn/HA	−0.86	1.8	5.9	0.11	87
Zn/HA + 0.01 g/lCS	−0.82	0.96	10.9	0.03	93
Zn/HA + 0.03 g/lCS	−0.78	0.79	15.7	0.02	94
Zn/HA + 0.05 g/lCS	−0.84	1.14	8.7	0.04	92

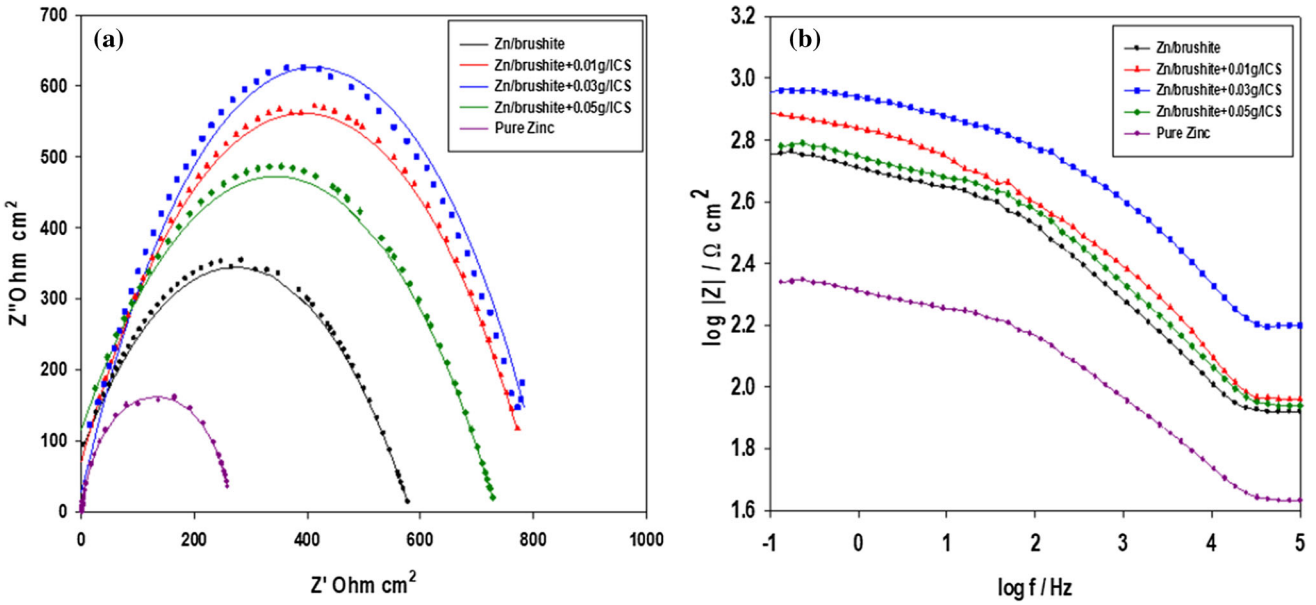

Figure 8 **a** Nyquist (symbols is experimental work and lines is fitting circuit) and **b** Bode plots of electrodeposited brushite and brushite / CS coatings on substrate in SBF solution at 37 °C.

the angular frequency in rad/s, and f is the frequency in Hz = S^{-1}. The outcomes of the EIS analysis are given in Table 4.

The following equation assesses the protection efficiency (PE %) provided by the nano composite coatings on the zinc substrate in SBF solution [63].

$$PE\% = 1 - R_p^{\circ}/R_p \times 100 \quad (12)$$

where R°_p and R_p are the resistances for both the uncoated and nanocomposite coatings, respectively.

Microwave heating produced a coating that was compact and thick, with good corrosion resistance for the zinc substrate. Potentiodynamic tests and EIS were utilized to estimate the protective effects of the resulting HA and HA/CS composite coatings. Compared with the electrodeposition method, the coating produced by microwave heating exhibited larger E_{corr} with smaller i_{corr} and larger charge transfer resistance R_p as represented in Fig. 11 and Fig. 12, respectively. The corrosion parameters resulting from

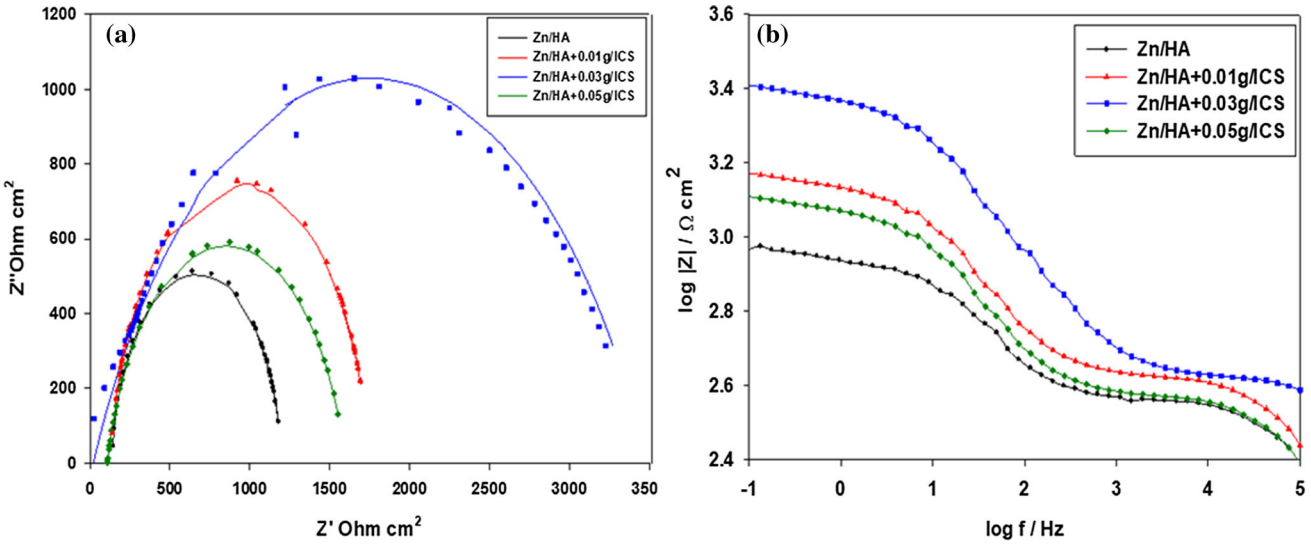

Figure 9 **a** Nyquist (symbols is experimental work and lines is fitting circuit) and **b** Bode plots for coated zinc after post treated in SBF solution at 37 °C.

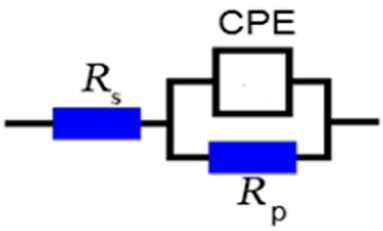

Figure 10 Equivalent circuits used for modelling of experimental EIS data.

the polarization curves are recorded in Table 3. Microwave provided a more uniform and denser coating with a large thickness compared to electrodeposition. The coating prevented SBF from penetrating the zinc substrate during implantation, resulting in good long-term corrosion resistance. The size of the capacitive loop grew in the Nyquist plots for the microwave method. The increase in capacitive loops and impedance denotes an enhancement in coating corrosion resistance, which is linked to

Table 4 Electrochemical impedance parameters

Sample	R_p/kΩ cm^2	CPE/μF cm^{-2}	α	Rs/Ω cm^2	PE%
Zinc	0.22	9.5	0.92	52	–
Zn/brushite	0.55	7.2	0.96	49	60
Zn/brushite + 0.01 g/lCS	0.82	4.2	0.86	29	73
Zn/brushite + 0.03 g/lCS	0.87	3.8	0.84	75	74
Zn/brushite + 0.05 g/lCS	0.72	6.4	0.86	86	69
Zn/HA	1.08	3.8	0.94	154	79
Zn/HA + 0.01 g/lCS	1.80	1.35	0.96	162	87
Zn/HA + 0.03 g/lCS	3.61	1.20	0.92	136	93
Zn/HA + 0.05 g/lCS	1.52	1.95	0.95	117	85
Microwave method					
Zn/HA	7.2	2.7	0.98	320	97
Zn/HA + 0.01 g/lCS	14.2	0.87	0.95	747	98
Zn/HA + 0.03 g/lCS	18	0.56	0.94	618	99
Zn/HA + 0.05 g/lCS	13.8	2	0.97	460	98

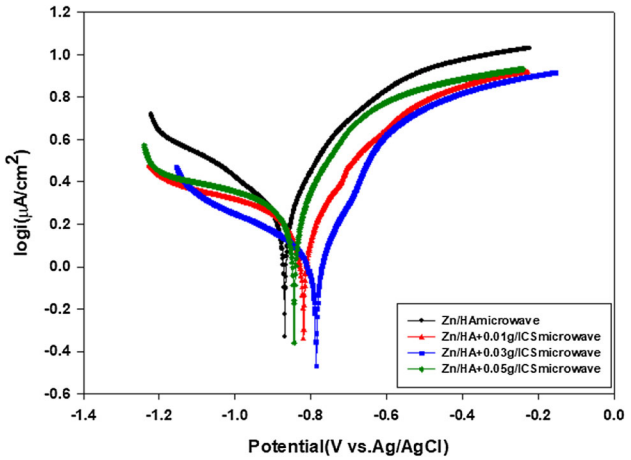

Figure 11 Potentiodynamic polarization curves of microwave deposition of HA and HA/CS coatings on Zn substrate in SBF solution at 37 °C.

crystallization. The proposed equivalent circuit for the EIS spectra is shown in Fig. 10, and the fitted values are presented in Table 4.

According to the model used in analysis, the effective capacitance can be calculated from the value of CPE (Q) and the coating resistance (R) by the following equation [65].

$$C_{\text{eff}} = Q^{1/\alpha}/R^{(1-\alpha)/\alpha} \tag{13}$$

The capacitance (C) of the coating film can related to the thickness using the well-known relation [65, 66]:

$$C_{\text{eff}} = \varepsilon_r \varepsilon_o A/d \tag{14}$$

where d is the coat thickness, ε_r the relative permittivity of the passive film, ε_o (8.85×10^{-12}F cm^{-1}) the permittivity of the vacuum and A the area in cm^2. Although the actual value of ε_r within the coat is difficult to estimate, a change in C can be utilized as an indicator for change in the film thickness (d) [67, 68]. Hence, the reciprocal capacitance of the coat is directly proportional to its thickness. From Table 4, it is clear that HA/CS(0.03 g/l) composite coatings prepared by microwave method offer a better protection efficiency.

A comparison of the corrosion performance offered by the HA/CS coated zinc substrate from the present work and similar coatings in literature data is given in Table 5.

Antibacterial activity and inhibition zone measurements

Using nutritional agar medium, the antibacterial activity of HA and HA/CS coatings was evaluated against staphylococcus aureus (a gram-positive bacteria). As seen in Table 6, both coatings exhibit better antibacterial activities in assessment to the standard reference drug ampicillin. The greater zone of inhibition indicates that the antimicrobial is more effective. After 24 h of incubation at 37 °C, both coatings showed zones of inhibition in the range of 26–32 mm, which is much better than the reference ampicillin (22 mm). The fact that HA/CS coatings had a larger zone of inhibition suggests that chitosan-based

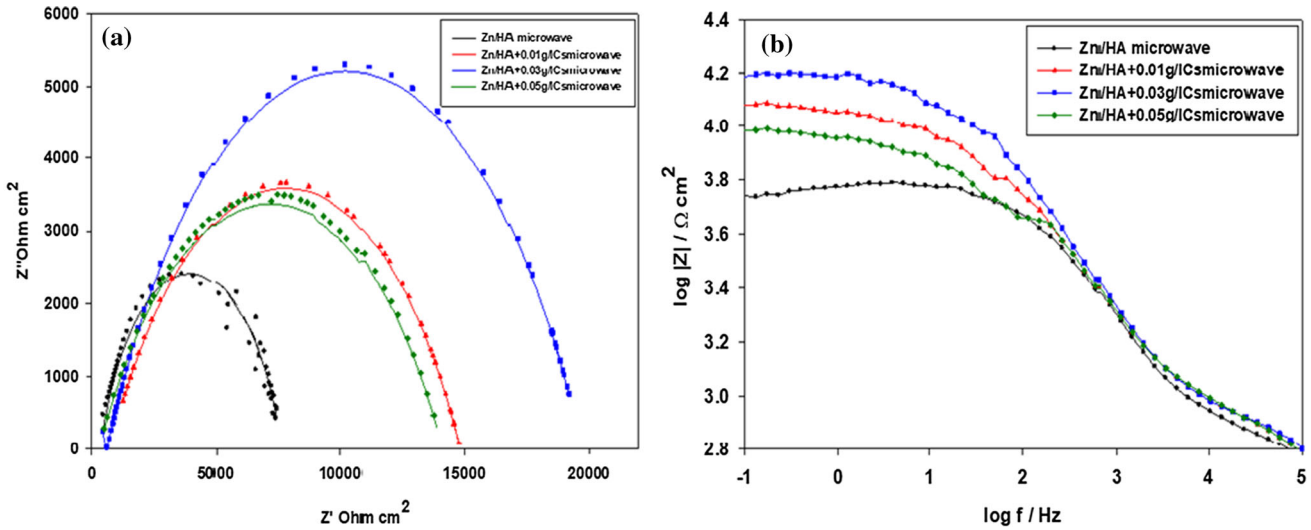

Figure 12 **a** Nyquist (symbols is experimental work and lines is fitting circuit) and **b** Bode plots of microwave deposition of HA and HA/CS coatings on Zn substrate in SBF solution at 37 °C.

Table 5 Corrosion parameters from potentiodynamic polarization curves of coated zinc substrate from the present work and literature data

Sample	Coating	Test medium	I_{corr}/μA/cm^2	E_{corr}/mV	Reference
Pure zinc	Chitosan dip-coating	Sodium sulphate	29.66	−883	[69]
Pure zinc	indigo carmine dip-coating	Sodium sulphate	14.38	−909	[37]
Pure zinc	Chitosan dip-coating	Sodium sulphate	15.56	−865	[38]
Pure zinc	Mg-based coating	Hank's solution	1.27	−1040	[70]
Pure zinc	Zinc phosphate dip-coating	Simulated body fluid (SBF)	8.16	−870	[71]
Pure zinc	Zinc phosphate/ alendronate dip-coating	Simulated body fluid (SBF)	7.78	−800	[71]
Pure zinc	Zinc phosphate immersion coating	Hank's solution	36	−973	[72]
Pure zinc	HA/CS electrodeposition method	Simulated body fluid (SBF)	1.1	−900	The present work
Pure zinc	HA/CS microwave method	Simulated body fluid (SBF)	0.79	−780	The present work

Table 6 In vitro antibacterial activity of HA and HA/CS coated zinc substrate against staphylococcus aureus for 24 h

Microorganism	HA coating	HA/Cs composite coating	Standard antibiotic ampicillin
Gram-positive bacteria Staphylococcus aureus	26 mm	32 mm	22 ± 0.1 mm

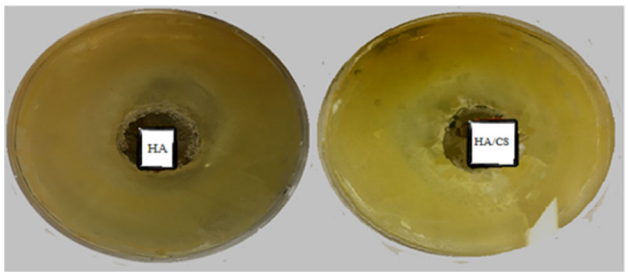

Figure 13 Zones of inhibition of the antibacterial activity.

composite coatings have a very high chance of stopping bacterial growth Fig. 13.

Recently, it was discovered that hydroxyapatite has improved biocompatibility and bone formation ability. The incorporation of chitosan in HA/CS composite coatings has the antibacterial ability to reduce the risk of bacterial contamination and post-operative infection. Therefore, HA/CS composite coatings are anticipated to be a promising zinc coating to enhance the biocompatibility for orthopedic bone applications. When compared to the electrodeposition method, microwave-assisted preparation of nano hydroxyapatite could be considered a fast, simple, inexpensive, and efficient method of coating preparation.

Conclusions

The following conclusion is reached based on the findings of this investigation:

1- Both the microwave-assisted method and the electrodeposition method were able to make HA and HA/CS coatings that were high quality and uniform.
2- X-ray diffraction analysis confirmed the formation of HA/CS composite coating on zinc substrate.
3- Based on polarization studies and electrochemical impedance measurements, the HA/CS composite coatings provided high corrosion resistance, the improvement being due to their action as a protective layer compared to the bare zinc substrate.
4- The HA and HA/CS coating offered better antibacterial activity against staphylococcus aureus
5- The results indicated that HA/CS composite coatings prepared by microwave can be considered a suitable biomaterial for use in implant applications.

Funding

Open access funding provided by The Science, Technology & Innovation Funding Authority (STDF) in cooperation with The Egyptian Knowledge Bank (EKB).

Declarations

Conflict of interest The authors declare that they have no conflict of interest.

References

[1] Meng Y, Liu L, Zhang D, Dong C, Yan Y, Volinsky AA, Wang L-N (2019) Initial formation of corrosion products on pure zinc in saline solution. Bioact mater 4:87–96

[2] Bowen PK, Drelich J, Goldman J (2013) Zinc exhibits ideal physiological corrosion behavior for bioabsorbable stents. Adv Mater 25:2577–2582

[3] Purnama A, Hermawan H, Mantovani D (2014) Biodegradable metal stents: a focused review on materials and clinical studies. J Biomater Tissue Eng 4:868–874

[4] Li H, Zheng Y, Qin L (2014) Progress of biodegradable metals. Prog Nat Sci Mater Int 24:414–422

[5] Frederickson CJ, Koh J-Y, Bush AI (2005) The neurobiology of zinc in health and disease. Nat Rev Neurosci 6:449–462

[6] Vojtěch D, Kubásek J, Šerák J, Novák P (2011) Mechanical and corrosion properties of newly developed biodegradable Zn-based alloys for bone fixation. Acta Biomater 7:3515–3522

[7] Zhang S, Zhang X, Zhao C, Li J, Song Y, Xie C, Tao H, Zhang Y, He Y, Jiang Y (2010) Research on an Mg–Zn alloy as a degradable biomaterial. Acta Biomater 6:626–640

[8] Jain D, Pareek S, Agarwala A, Shrivastava R, Sassi W, Parida SK, Behera D (2021) Effect of exposure time on corrosion behavior of zinc-alloy in simulated body fluid solution: electrochemical and surface investigation. J Mater Res Technol 10:738–751

[9] Murni N, Dambatta M, Yeap S, Froemming G, Hermawan H (2015) Cytotoxicity evaluation of biodegradable Zn–3Mg alloy toward normal human osteoblast cells. Mater Sci Eng C 49:560–566

[10] Moravej M, Mantovani D (2011) Biodegradable metals for cardiovascular stent application: interests and new opportunities. Int J Mol Sci 12:4250–4270

[11] Kuhlmann J, Bartsch I, Willbold E, Schuchardt S, Holz O, Hort N, Höche D, Heineman WR, Witte F (2013) Fast escape of hydrogen from gas cavities around corroding magnesium implants. Acta Biomater 9:8714–8721

[12] Staiger MP, Pietak AM, Huadmai J, Dias G (2006) Magnesium and its alloys as orthopedic biomaterials: a review. Biomaterials 27:1728–1734

[13] Chen J, Tan L, Yang K (2017) Effect of heat treatment on mechanical and biodegradable properties of an extruded ZK60 alloy. Bioact mater 2:19–26

[14] Schinhammer M, Hänzi AC, Löffler JF, Uggowitzer PJ (2010) Design strategy for biodegradable Fe-based alloys for medical applications. Acta Biomater 6:1705–1713

[15] Schinhammer M (2012) Development and characterization of biodegradable Fe-based alloys for temporary medical applications, in, ETH Zurich, viii–xiii

[16] Cheng J, Liu B, Wu Y, Zheng Y (2013) Comparative in vitro study on pure metals (Fe, Mn, Mg, Zn and W) as biodegradable metals. J Mater Sci Technol 29:619–627

[17] Yanovska G, Bolshanina SB, Kuznetsov V (2017) Formation of hydroxyapatite coatings with addition of chitosan from aqueous solutions by thermal substrate method. J eng sci, F1-F4

[18] Furko M, Horváth ZE, Sulyok A, Kis VK, Balázsi K, Mihály J, Balázsi C (2021) Preparation and morphological investigation on bioactive ion-modified carbonated hydroxyapatite-biopolymer composite ceramics as coatings for orthopaedic implants. Ceram Int 48(1):760–768

[19] Park KH, Kim S-J, Hwang M-J, Song H-J, Park Y-J (2017) Pulse electrodeposition of hydroxyapatite/chitosan coatings on titanium substrate for dental implant. Colloid Polym Sci 295:1843–1849

[20] Dorozhkin SV, Epple M (2002) Biological and medical significance of calcium phosphates. Angew Chem Int Ed 41:3130–3146

[21] Suzuki O, Imaizumi H, Kamakura S, Katagiri T (2008) Bone regeneration by synthetic octacalcium phosphate and its role in biological mineralization. Curr Med Chem 15:305–313

[22] Zhang F, Cai S, Xu G, Wang F, Yu N, Ling R, Wu X (2016) Preparation and bioactivity of apatite coating on Ti6Al4V alloy by microwave assisted aqueous chemical method. Ceram Int 42:18466–18473

[23] Shoeib M (2004) Beschichtung von verbundwerkstoffen mit hydroxylapatit: anwendungen in der medizin-und biotechnologie. Galvanotechnik 95:1860–1867

[24] kumar Balu S, Andra S, Jeevanandam J, Vidyavathy SM, Sampath V (2021) Emerging marine derived nanohydroxyapatite and their composites for implant and biomedical applications. J Mech Behav Biomed Mat 119:104523

[25] Bartmański M, Pawłowski Ł, Belcarz A, Przekora A, Ginalska G, Strugała G, Cieślik BM, Pałubicka A, Zieliński A (2021) The chemical and biological properties of nanohydroxyapatite Coatings with antibacterial nanometals, obtained in the electrophoretic process on the Ti13Zr13Nb alloy. Int J Mol Sci 22:3172

[26] Neacsu IA, Arsenie LV, Trusca R, Ardelean IL, Mihailescu N, Mihailescu IN, Ristoscu C, Bleotu C, Ficai A, Andronescu E (2019) Biomimetic collagen/Zn2+-Substituted calcium phosphate composite coatings on titanium substrates as prospective bioactive layer for implants: a comparative study spin coating vs. MAPLE. Nanomaterials 9:692

[27] Kar A, Raja K, Misra M (2006) Electrodeposition of hydroxyapatite onto nanotubular TiO2 for implant applications. Surf Coat Technol 201:3723–3731

[28] Yusoff MFM, Kasim NHA, Himratul-Aznita WH, Saidin S, Genasan K, Kamarul T, Radzi Z (2021) Physicochemical, antibacterial and biocompatibility assessments of silver incorporated nano-hydroxyapatite synthesized using a novel microwave-assisted wet precipitation technique. Mater Charact 178:111169

[29] Hassan MN, Mahmoud MM, Abd El-Fattah A, Kandil S (2016) Microwave-assisted preparation of nano-hydroxyapatite for bone substitutes. Ceram Int 42:3725–3744

[30] Şimsek Y, Avci Ş (2019) Synthesis and characterization of hydroxyapatite produced by microwave assisted precipitation technique. Acta Phys Pol A 135:974–976

[31] Demirtaş TT, Kaynak G, Gümüşderelioğlu M (2015) Bone-like hydroxyapatite precipitated from 10× SBF-like solution by microwave irradiation. Mater Sci Eng C 49:713–719

[32] Vandecandelaere N, Rey C, Drouet C (2012) Biomimetic apatite-based biomaterials: on the critical impact of synthesis and post-synthesis parameters. J Mater Sci Mater Med 23:2593–2606. https://doi.org/10.1007/s10856-012-4719-y

[33] Sheikh Z, Najeeb S, Khurshid Z, Verma V, Rashid H, Glogauer M (2015) Biodegradable materials for bone repair and tissue engineering applications. Materials 8:5744–5794

[34] Bartmański M, Pawłowski Ł, Mielewczyk-Gryń A, Strugała G, Rokosz K, Gaiaschi S, Chapon P, Raaen S, Zieliński A (2021) The influence of nanometals, dispersed in the electrophoretic nanohydroxyapatite coatings on the ti13zr13nb alloy, on their morphology and mechanical properties. Materials 14:1638

[35] Hu H, Lin C, Hu R, Leng Y (2002) A study on hybrid bioceramic coatings of HA/poly (vinyl acetate) co-deposited electrochemically on Ti–6Al–4V alloy surface. Mater Sci Eng C 20:209–214

[36] Park K, Kim S, Hwang M, Song H, Park Y (2017) Biomimetic fabrication of calcium phosphate/chitosan nanohybrid composite in modified simulated body fluids. Express Polym Lett 11:14–20

[37] Szőke ÁF, Szabó GS, Hórvölgyi Z, Albert E, Gaina L, Muresan LM (2019) Eco-friendly indigo carmine-loaded chitosan coatings for improved anti-corrosion protection of zinc substrates. Carbohyd Polym 215:63–72

[38] Szőke ÁF, Szabó GS, Hórvölgyi Z, Albert E, Végh AG, Zimányi L, Muresan LM (2020) Accumulation of 2-Acetylamino-5-mercapto-1, 3, 4-thiadiazole in chitosan coatings for improved anticorrosive effect on zinc. Int J Biol Macromol 142:423–431

[39] Wang J, de Boer J, De Groot K (2004) Preparation and characterization of electrodeposited calcium phosphate/chitosan coating on Ti6Al4V plates. J Dent Res 83:296–301

[40] Boccaccini A, Keim S, Ma R, Li Y, Zhitomirsky I (2010) Electrophoretic deposition of biomaterials. J R Soc Interface 7:S581–S613

[41] Shalaby HA, Hashem AM, Badr NA, Shoeib MM, Khafagy MG (2011) Preparation of ordered nano-titania arrays and electrodeposition of nano-hydroxyapatite crystals on Ti-6Al%-4% V dental implant surfaces. J Am Sci 7:574–584

[42] Abdeltawab A, Shoeib M, Mohamed S (2011) Electrophoretic deposition of hydroxyapatite coatings on titanium from dimethylformamide suspensions. Surf Coat Technol 206:43–50

[43] DileepKumar V, Sridhar MS, Aramwit P, Krut'ko VK, Musskaya ON, Glazov IE, Reddy N (2021) A Review on the Synthesis and Properties of hydroxyapatite for biomedical applications. J Biomater Sci Polymer Ed 33:1–29

[44] Abd El-Salam H, Abd El-Hafez G, Askalany H, Fekry A (2020) A creation of poly (N-2-hydroxyethylaniline-co-2-chloroaniline) for corrosion control of mild steel in acidic medium. J Bio- Tribo- Corros 6:1–14

[45] Abdel-Gawad SA, Sadik MA, Shoeib MA (2019) Preparation and properties of a novel nano Ni-B-Sn by electroless

deposition on 7075–T6 aluminum alloy for aerospace application. J Alloy Compd 785:1284–1292

[46] S. Sathiyanarayanan, C. Marikkannu, P.B. Srinivasan, V. Muthupandi (2002) Corrosion behaviour of Ti6Al4V and duplex stainless steel (UNS31803) in synthetic bio-fluids. Anti-Corros Methods Mater

[47] Francis A, Abdel-Gawad S, Shoeib M (2021) Toward CNT-reinforced chitosan-based ceramic composite coatings on biodegradable magnesium for surgical implants. J Coat Technol Res 18:1–18

[48] Abdel-Gawad SA, Shoeib MA (2019) Corrosion studies and microstructure of Mg−Zn−Ca alloys for biomedical applications. Surf Interfaces 14:108–116

[49] Redepenning J, Venkataraman G, Chen J, Stafford N (2003) Electrochemical preparation of chitosan/hydroxyapatite composite coatings on titanium substrates, journal of biomedical materials research part a: an official journal of the society for biomaterials, the japanese society for biomaterials, and the australian society for biomaterials and the korean society for. Biomaterials 66:411–416

[50] Awasthi S, Pandey SK, Arunan E, Srivastava C (2021) A review on hydroxyapatite coatings for the biomedical applications: experimental and theoretical perspectives. J Mater Chem B 9:228–249

[51] Yi H, Wu LQ, Ghodssi R, Rubloff GW, Payne GF, Bentley WE (2004) A robust technique for assembly of nucleic acid hybridization chips based on electrochemically templated chitosan. Anal Chem 76:365–372

[52] Wang X, Du Y, Liu H (2004) Preparation, characterization and antimicrobial activity of chitosan–Zn complex. Carbohyd Polym 56:21–26

[53] Bartkowiak A, Hunkeler D (1999) Alginate–oligochitosan microcapsules: a mechanistic study relating membrane and capsule properties to reaction conditions. Chem Mater 11:2486–2492

[54] Pang X, Zhitomirsky I (2005) Electrodeposition of composite hydroxyapatite–chitosan films. Mater Chem Phys 94:245–251

[55] Nikpour M, Rabiee S, Jahanshahi M (2012) Synthesis and characterization of hydroxyapatite/chitosan nanocomposite materials for medical engineering applications. Compos B Eng 43:1881–1886

[56] Shen S, Cai S, Zhang M, Xu G, Li Y, Ling R, Wu X (2015) Microwave assisted deposition of hydroxyapatite coating on a magnesium alloy with enhanced corrosion resistance. Mater Lett 159:146–149

[57] Ban S, Hasegawa J (2002) Morphological regulation and crystal growth of hydrothermal-electrochemically deposited apatite. Biomaterials 23:2965–2972

[58] Viswanath B, Ravishankar N (2008) Controlled synthesis of plate-shaped hydroxyapatite and implications for the morphology of the apatite phase in bone. Biomaterials 29:4855–4863

[59] Haque E, Khan NA, Kim CM, Jhung SH (2011) Syntheses of metal-organic frameworks and aluminophosphates under microwave heating: quantitative analysis of accelerations. Cryst Growth Des 11:4413–4421

[60] Hahn B-D, Park D-S, Choi J-J, Ryu J, Yoon W-H, Choi J-H, Kim H-E, Kim S-G (2011) Aerosol deposition of hydroxyapatite–chitosan composite coatings on biodegradable magnesium alloy. Surf Coat Technol 205:3112–3118

[61] Huang S, Wu W, Su Y, Qiao L, Yan Y (2021) Insight into the corrosion behaviour and degradation mechanism of pure zinc in simulated body fluid. Corros Sci 178:109071

[62] Gawad SA, Nasr A, Fekry AM, Filippov LO (2021) Electrochemical and hydrogen evolution behaviour of a novel nano-cobalt/nano-chitosan composite coating on a surgical 316L stainless steel alloy as an implant. Int J Hydrog Energy 46:18233–18241

[63] Abdel-Gawad SA, Sadik MA, Shoeib MA (2018) Enhancing corrosion resistance of galvanized steel by phosphating and silicate post–sealing. Int J Electrochem Sci 13:2688–2704

[64] Nasr A, Gawad SA, Fekry AM (2020) A sensor for monitoring the corrosion behavior of orthopedic drug calcium hydrogen phosphate on a surgical 316L stainless steel alloy as implant. J Bio- Tribo- Corros 6:1–10

[65] Hirschorn B, Orazem ME, Tribollet B, Vivier V, Frateur I, Musiani M (2010) Determination of effective capacitance and film thickness from constant-phase-element parameters. Electrochim Acta 55:6218–6227

[66] Heakal FE-T, Fekry A, Ghoneim A (2008) Corrosion characterization of new tin–silver binary alloys in nitric acid solutions. Corros Sci 50:1618–1626

[67] Heakal FE-T, Fekry A, Jibril MAE-B (2011) Electrochemical behaviour of the Mg alloy AZ91D in borate solutions. Corros Sci 53:1174–1185

[68] Ghoneim A, Mogoda A, Awad KA, Heakal F (2012) Electrochemical studies of titanium and its Ti–6Al–4V alloy in phosphoric acid solutions. Int J Electrochem Sci 7:6539–6554

[69] Szőke ÁF, Szabó G, Simó Z, Hórvölgyi Z, Albert E, Végh AG, Zimányi L, Muresan LM (2019) Chitosan coatings

ionically cross-linked with ammonium paratungstate as anticorrosive coatings for zinc. Eur Polymer J 118:205–212

[70] Zhu M, Lu Y, Zhang C, Li L, Xie M, Lin J, Tang K (2019) Facile fabrication of Mg-based coating to improve the biodegradable behavior and cytocompatibility of pure zinc. Surf Coat Technol 372:209–217

[71] Mo X, Qian J, Chen Y, Zhang W, Xian P, Tang S, Zhou C, Huang N, Ji H, Luo E (2021) Corrosion and degradation decelerating alendronate embedded zinc phosphate hybrid coating on biodegradable Zn biomaterials. Corros Sci 184:109398

[72] Su Y, Yang H, Gao J, Qin YX, Zheng Y, Zhu D (2019) Interfacial zinc phosphate is the key to controlling biocompatibility of metallic zinc implants. Adv Sci 6:1900112